AGU ADVANCING EARTH AND SPACE SCIENCE

Geophysical Research Letters®

RESEARCH LETTER
10.1029/2021GL093833

Key Points:

- The majority of effective radiative forcing in HadGEM3-GA7.1 comes from stratocumulus clouds
- Forcing from marine stratocumulus clouds is highly sensitive to aerosol perturbations
- Decomposing radiative forcing by cloud regimes can be a useful technique to gain insights into climate model predictions

Supporting Information:

Supporting Information may be found in the online version of this article.

Correspondence to:

T. Langton,
thomas.langton@physics.ox.ac.uk

Citation:

Langton, T., Stier, P., Watson-Parris, D., & Mulcahy, J. P. (2021). Decomposing effective radiative forcing due to aerosol cloud interactions by global cloud regimes. *Geophysical Research Letters*, *48*, e2021GL093833. https://doi.org/10.1029/2021GL093833

Received 28 APR 2021
Accepted 14 AUG 2021

Decomposing Effective Radiative Forcing Due to Aerosol Cloud Interactions by Global Cloud Regimes

Tom Langton[1], Philip Stier[1], Duncan Watson-Parris[1], and Jane P. Mulcahy[2]

[1]Atmospheric, Oceanic and Planetary Physics, Department of Physics, University of Oxford, Oxford, UK, [2]Met Office, Exeter, UK

Abstract Quantifying effective radiative forcing due to aerosol-cloud interactions ($EERF_{ACI}$) remains a largely uncertain process, and the magnitude remains unconstrained in general circulation models. Previous studies focus on the magnitude of ERF_{ACI} arising from all cloud types, or examine it in the framework of dynamical regimes. Aerosol forcing due to aerosol-cloud interactions in the HadGEM3-GA7.1 global climate model is decomposed into several global observational cloud regimes. Regimes are assigned to model gridboxes and forcing due to aerosol-cloud interactions is calculated on a regime-by-regime basis with a 20-year averaging period. Patterns of regime occurrence are in good agreement with satellite observations. ERF_{ACI} is then further decomposed into three terms, representing radiative changes within a given regime, transitions between different cloud regimes, and nonlinear effects. The total global mean ERF_{ACI} is $-1.03\ Wm^{-2}$. When decomposed, simulated ERF_{ACI} is greatest in the thick stratocumulus regime ($-0.51\ Wm^{-2}$).

Plain Language Summary The effect of anthropogenic aerosol emissions on clouds is highly uncertain in climate models. Many previous attempts to reduce this uncertainty have focused on examining all cloud types as a whole. This work sets out a framework to examine one measure of aerosol-cloud interactions when the effect is split by different cloud types. This framework is applied to the HadGEM3-GA7.1 climate model. It is found that thick stratocumulus clouds exhibit the strongest aerosol-cloud interactions, especially those found off the west coast of both North and South America, and West Africa. It is hoped that this will lead to a greater understanding of how these interactions manifest themselves in different cloud types, and that this methodology will promote the use of constraints on specific cloud types, to provide potentially greater reductions in the aforementioned uncertainty.

1. Introduction

The radiative forcing (RF) produced by aerosol remains a large source of uncertainty in climate models (IPCC, 2013). General Circulation Models (GCMs) show a wide range in their predictions of aerosol forcing, through the uncertainty in effective radiative forcing, due to aerosol-cloud interactions (ERF_{ACI})(Bellouin et al., 2020).

Aerosol-cloud interactions are driven by a number of different effects, occurring on different timescales. Instantaneous effects will drive changes in the instantaneous radiative forcing due to aerosol-cloud interactions (RF_{ACI}). For instance, the Twomey effect predicts that a cloud with constant liquid water content will increase in optical depth when aerosol loading increases (Twomey, 1977). Effects that occur over longer timescales will instead affect the ERF_{ACI}, for instance the 2nd indirect effect (Albrecht, 1989) predicts that aerosol leads to increased liquid water path and cloud lifetime (Rotstayn, 1999). These effects are difficult to constrain however, due to the need for parameterization in GCMs owing to the microscopic nature of aerosol-cloud interactions, the huge heterogeneity in aerosol loading, and the uncertainty in the exact nature of these mechanisms themselves (Boucher et al., 2013).

Even within GCMs, the indirect forcing by aerosol can vary wildly. As can be seen in Mulcahy et al. (2018), the change in forcing due to aerosol-cloud interactions (ERF_{ACI}) between the GA7.0 and GA7.1 (Global Atmosphere) science configurations of HadGEM3 (Hadley Center Global Environmental Model version 3) was $1.04\ Wm^{-2}$. As a result, it remains a question as to exactly why these changes can bring about such large variation in ERF_{ACI}, and which types of cloud are the most sensitive to these changes in the model. One way to do this is to examine the ERF_{ACI} when it is decomposed into cloud regimes. This will also give a detailed

insight into the way cloud processes are modeled, and provides a pathway to incorporate results from observations and high resolution modeling, as these will make predictions relating to specific cloud regimes.

Regime-based analysis of clouds uses joint histograms of cloud top pressure (CTP) and cloud optical depth (COD), and was pioneered by Jakob and Tselioudis (2003), using the data produced by the International Satellite Cloud Climatology Project (ISCCP [Rossow & Schiffer, 1999]). This analysis has had success when applied to observations. For instance, several studies have determined the sensitivity of different cloud properties to AOD in a regime-based framework (Gryspeerdt & Stier, 2012; Oreopoulos et al., 2020). In addition, Schuddeboom et al. (2018) examined differences in the cloud radiative effect (CRE) between models and observations. What has not been done, however, is to examine on a regime-by-regime basis the indirect radiative forcing by aerosol. It is reasonable to believe, in light of these papers, that different cloud regimes may react differently to an increase in aerosol emissions, and hence have varying total contributions to the aerosol forcing. When decomposed into regimes, it will also be possible to examine the modeled sensitivities of each regime, for instance the sensitivity of cloud albedo to aerosol loading.

This paper sets out a framework to analyze indirect aerosol forcing by cloud regime, and applies this methodology to analyze the forcing from HadGEM3. This methodology can provide useful insights into how different models calculate aerosol processes. In addition, the forcing can be quantified in terms of changes in the average properties of each regime, and also to account for differing relative frequency of occurence (RFO) of regimes between present-day and preindustrial time periods.

2. Methodology

2.1. Model and Experimental Design

This study makes use of 2 different model runs of HadGEM3 GA7.1 global model and the Global Land configuration version 7.1 (GL7.1) (Walters et al., 2019). A 20-year run is performed for both a present-day (1988–2008) and preindustrial (1850 emissions) time period, both at N96 resolution ($1.875° \times 1.25°$) with 85 vertical levels. The aerosol-cloud interactions are handled by the Unified Model Physics scheme, described in Mulcahy et al. (2018). Cloud droplet number concentrations are diagnosed by the UK Chemistry and Aerosol model, using the Global Model of Aerosol Processes (GLOMAP-mode) (Mann et al., 2010) coupled to the PC2 cloud scheme with the Wilson and Ballard microphysics scheme (Wilson et al., 2008; Wilson & Ballard, 1999), via the Abdul-Razzak Ghan activation scheme (Abdul-Razzak & Ghan, 2000) as described in West et al. (2014). The emissions used are the present day Coupled Model Intercomparison Project Phase 6 (CMIP6) emissions data sets (Hoesly et al., 2018). For the 1850 emissions, anthropogenic aerosol emissions were reverted to their preindustrial estimates, while natural emissions, sea ice coverage, and sea surface temperatures were kept identical to the present day run.

The CFMIP Observational Simulator Package (COSP; Bodas-Salcedo et al. [2011]) is used to generate model simulations of the joint histograms of CTP and COD (τ) available from the ISCCP D1 products (Rossow & Schiffer, 1999). As COSP is designed to mimic the output of ISCCP, these histograms are only available on sunlit points.

Data are generated at every radiation time step (1 h), and regimes can be assigned on daylit points only. As COSP only produces data on daylit points, the nighttime LW forcing is calculated for all cloud types, and then divided amongst the regimes proportionally to their daytime RFO.

The Wilson and Ballard cloud microphysics scheme does not include interactions between aerosol and either the convective or ice microphysics, however, there are interactions between convective clouds and the large-scale microphysics, as condensate is detrained from the convective cloud into the large-scale cloud, affecting cloud liquid and ice water content. This means that while aerosols in the region of deep convective regimes will not directly interact with the clouds as they would in an LES model, they will produce a signal, although this signal could be difficult to interpret accurately.

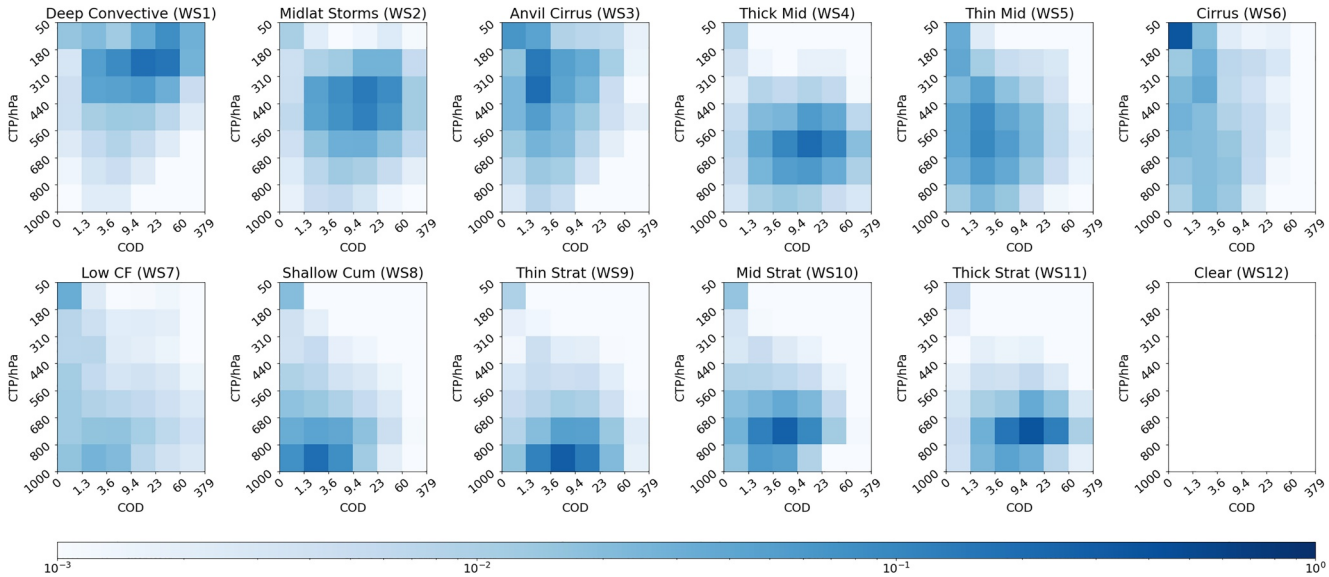

Figure 1. Histograms showing the 12 cluster centroids used in this analysis, as taken from Tselioudis et al. (2013). Shading represents cloud fraction (CF). The clear regime was assigned by clustering on the other 11 regimes, and then applying a CF-dependent mask to the gridboxes. The three different stratocumulus regimes were all merged into one cluster post-allocation.

2.2. Regime Assignment

Cloud regime definitions were taken from the work of Tselioudis et al. (2013), which defined a set of 11 (Global) Weather States (WS) from ISCCP observations using a k-means clustering algorithm (Anderberg, 2014), which clusters on 6×7 joint histograms of cloud top pressure (CTP) and cloud optical depth (COD). These are depicted visually in Figure 1. The average properties of each of these centroids, which are used for regime assignment, are shown in Table S1.

These cloud regimes can be seen to somewhat mimic classical cloud types. Gridboxes with CF $\leq 0.5\%$ are assigned to a separate clear-sky regime. In this analysis, several regimes with similar geographical distributions and cloud vertical structures are merged together. This is done by first assigning the regimes to the original 11 weather states defined by Tselioudis et al. (2013), and then not distinguishing between the merged states. These merged states are:

1. Anvil Cirrus (WS3) & Cirrus (WS6) $\rightarrow$ Cirrus
2. Shallow Cumulus (WS8) & Thin Strat (WS9) $\rightarrow$ Thin Stratocumulus
3. Mid Strat (WS10) & Thick Strat (WS11) $\rightarrow$ Thick Stratocumulus

This method has the advantage that the ERF_{ACI} of regimes with a low RFO appears amplified by grouping together physically similar regimes (e.g., Cirrus and Anvil Cirrus), without changing the initial cluster definitions.

Cloud regimes are assigned based on the methodology of Williams and Webb (2009). The joint CTP-τ histograms produced by COSP vary slightly from the observational histograms, as the bottom COD bin ($\tau < 1.3$) is split into two, making a 7×7 joint histogram. These new bins are $\tau < 0.3$ and $0.3 < \tau < 1.3$. These CTP-τ histograms are averaged according to their bin-center values to obtain a vector containing gridbox-mean values of CTP, albedo (α), and CF. Albedo values are taken from Williams and Webb (2009), which converts COD to α using the conversion table within the ISCCP simulator code, and then uses linear interpolation to get bin-center values of α. The bottom two model bins are kept separate, while a bin-center value for the satellite histograms was determined using further linear interpolation. The gridboxes are then assigned a regime by determining the centroid with the minimum Euclidean distance to this vector.

2.3. Aerosol Forcing by Cloud Regime

2.3.1. Definitions

In this paper, we examine the indirect effects of aerosol on clouds, as modeled by the Wilson and Ballard single moment cloud microphysics scheme within HadGEM3. All functions unless stated otherwise are assumed to be functions of latitude and longitude, and will have these arguments omitted for conciseness.

Following the methods and terminology of Ghan (2013), we define the cloud radiative forcing due to aerosols (ΔC_{clean}) as:

$$\Delta C_{\text{clean}} = \Delta(F_{\text{clean}} - F_{\text{clear,clean}}) \tag{1}$$

where Δ denotes the difference between present-day and preindustrial emissions periods, C_{clean} denotes the clean-cloud radiative effect, F denotes the net top-of-atmosphere (TOA) radiative flux, the difference between incoming and outgoing flux for both SW and LW radiation, and subscripts clean & clear denote the TOA fluxes when the model removes the direct radiative effects of aerosol and cloud, respectively.

Relative frequency of occurrence of the kth cloud regime is denoted by $R^k(T)$, and we denote present-day and preindustrial time periods by T_1 and T_0 respectively. Finally, the cloud radiative effect of the kth regime during time period T, $C^k(T)$ is calculated as:

$$C^k(T) = \frac{\sum_{t \in T} C(t)\delta_{R(t),k}}{\sum_{t \in T} \delta_{R(t),k}} \tag{2}$$

where $R(t)$ is a discrete 10-valued function indicating which cloud regime is seen in each gridbox, δ is the Kronecker delta, and the sum is performed over all time steps t in the model run representing time period T. $R(t)$ references the cloud regimes post-merge, rather than the 12 observational regimes found in (Tselioudis et al., 2013).

2.3.2. Calculation

It must be possible to recover total clean cloud forcing ERF_{ACI} simply by summing over each regime. ERF_{ACI} is decomposed into a contribution by each regime so that it can be written out as:

$$\Delta C_{\text{clean}} = \sum_k R^k(T_1)C^k(T_1) - R^k(T_0)C^k(T_0) \tag{3}$$

Having done this, it makes sense to define the total forcing by each cloud regime $\Delta C^k_{\text{clean}}$, to be the summand of Equation 3. However, this definition is a little nonphysical and it makes more sense to further break down the forcing into individual effects. These proposed effects are:

1. Total forcing resulting from the mean properties within each cloud regime changing, ΔC^k_α.
2. Total forcing resulting from the changing RFO of each cloud regime, ΔC^k_{RFO}.
3. Any additional terms required to recover Equation 3, representing nonlinear interactions.

Therefore, defining $\Delta R^k = R^k(T_1) - R^k(T_0)$, and analogously $\Delta C^k = C^k(T_1) - C^k(T_0)$, this becomes:

$$\Delta C^k_\alpha = R^k(T_0)\Delta C^k \tag{4}$$

$$\Delta C^k_{\text{RFO}} = C^k(T_0)\Delta R^k \tag{5}$$

$$\Delta C^k_{\text{clean}} = \Delta C^k_\alpha + \Delta C^k_{\text{RFO}} + \Delta R^k \Delta C^k \tag{6}$$

$$= R^k(T_0)\Delta C^k + C^k(T_0)\Delta R^k + \Delta R^k \Delta C^k \tag{7}$$

Multiplying out the terms of $\Delta C^k_{\text{clean}}$ and summing over k, one eventually recovers the expression given in Equation 3.

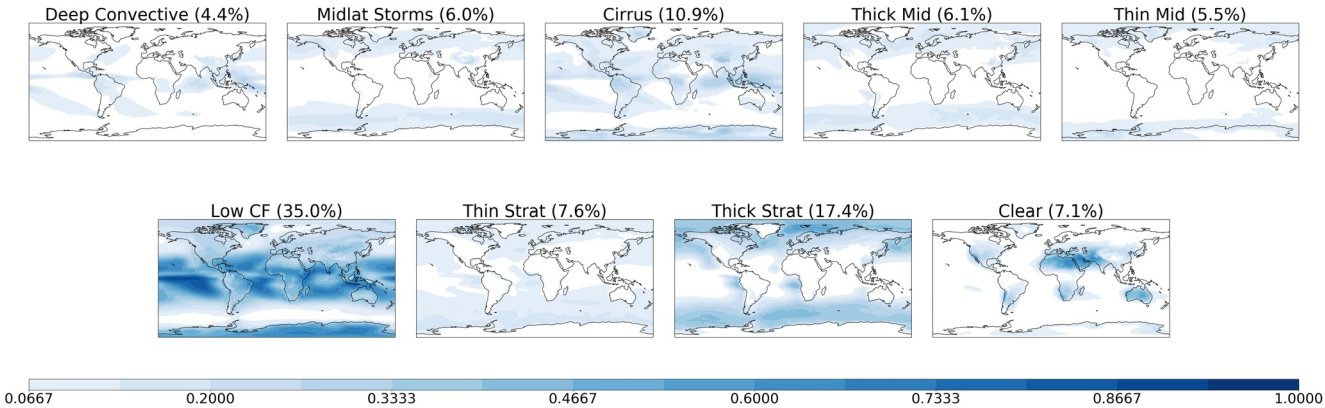

Figure 2. HadGEM simulated relative frequency of occurrence of each of the cloud regimes defined in this figure in the present-day simulation, including the clear-sky regime, assigned to gridboxes with $CF \leq 0.5\%$.

3. Results

Figure 2 shows the RFO of the 9 regimes used in the analysis in the present-day simulation. This shows that HadGEM3 broadly reproduces the satellite retrieved patterns seen in Tselioudis et al. (2013) throughout the tropics, especially in the cases of deep convection and the low CF regime, which represents regimes with a mixture of shallow cumulus and cirrus clouds. The k-means algorithm also does a good job distinguishing between storms seen in the ITCZ (WS1) and those in the midlatitudes (WS2). The dominant cloud regimes are the low CF regime, and the thick stratocumulus regime, primarily seen over the southern ocean and in the marine stratocumulus regions off the west coasts of Africa, North, and South America. The model fails to reproduce the very high observational RFO of the thick stratocumulus regimes seen in marine stratocumulus decks. Similarly, thin stratocumulus/shallow cumulus clouds are globally underrepresented, particularly over equatorial landmasses. This indicates that the model has difficulty simulating very thin cloud. The clear-sky regime is also over-represented by 5.2% globally, lending further evidence to this conclusion.

Figure S3 shows the increase in CCN at cloud base between PD and PI simulations. CCN is defined by the dry particle cutoff radius being larger than 50 nm. The strongest increase is seen over land, predominantly over China and south-east Asia, and the Indian subcontinent, with other more localized perturbations seen elsewhere over areas with high emissions. The Southern ocean sees very little aerosol perturbation, and the north Atlantic and Pacific see a perturbation an order of magnitude smaller than the one seen over land.

Figure 3 shows the total forcing produced by each cloud regime before any decomposition into individual effects, $\Delta C^{k}_{\text{clean}}$. This figure shows that approximately 50% of the total forcing comes from the thick stratocumulus regime.

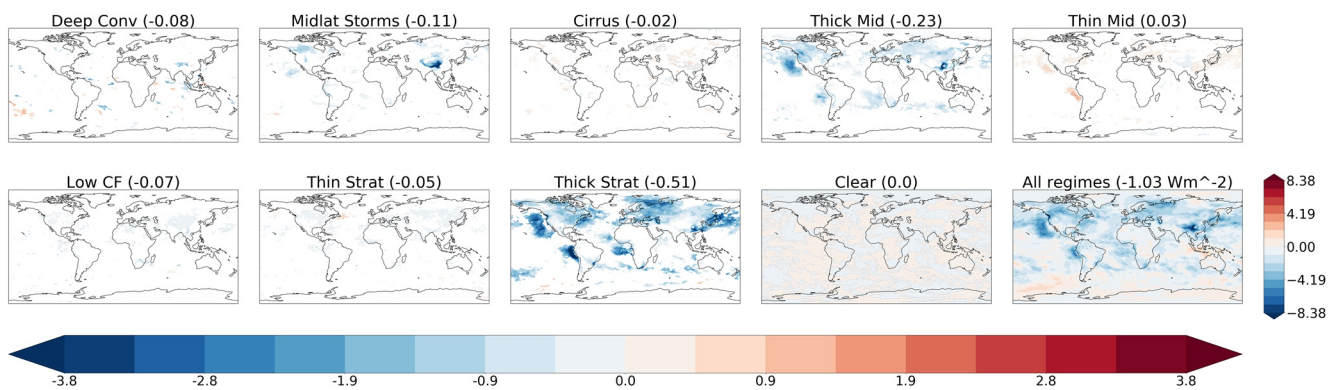

Figure 3. Total indirect aerosol forcing arising from each cloud regime, $\Delta C^{k}_{\text{clean}}$.

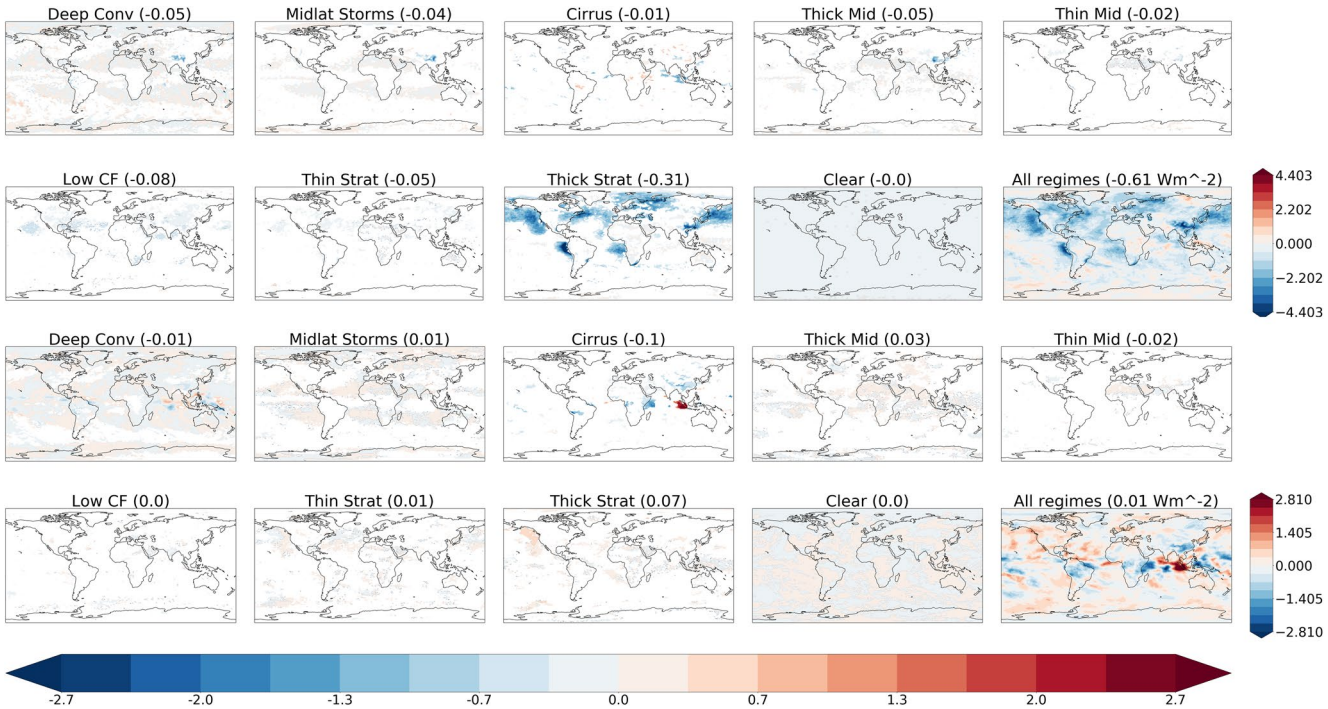

Figure 4. Indirect aerosol forcing arising from changes in regime mean properties for both shortwave (top) and longwave (bottom), ΔC_{α}^{k}. The horizontal colorbar shows values for each individual regime, while the vertical colorbar shows values for all regimes combined.

Figure 4 shows both shortwave and longwave contributions to the forcing produced by changes to mean properties of each cloud regime, as given in Equation 4. The data are aggregated for each month, and then subjected to a 2-tailed *t*-test. The data shown are significant at the 5% level. The forcing is dominated by the shortwave contribution by the thick stratocumulus regime, particularly in the marine stratocumulus decks off the coast of Africa and North & South America, and in the north Pacific and north Atlantic shipping lanes. The longwave contribution is much smaller than the shortwave, and is more pronounced in regimes with high CF, for instance the thick stratocumulus or thick midlevel cloud regimes. As the cloud fraction in the merged thick stratocumulus regime is already very high, it is likely that this forcing is arising from an increase in optical thickness of these clouds.

The Cirrus regime shows almost no shortwave forcing, however, it does present the highest longwave forcing of all regimes ($-0.10\ \mathrm{Wm}^{-2}$).

Figure 5 shows the shortwave and longwave contributions to the forcing produced by changes in occurrence of each cloud regime. Once again, this effect is dominated by the shortwave contribution, this time with a roughly equal weighting between the thick midlevel and thick stratocumulus regimes for both SW and LW radiation. Because of the predominantly negative sign of cloud radiative effects, it is easy to see how changes in RFO manifest themselves in forcings. An increased RFO of a particular regime, broadly speaking, will result in an increased negative shortwave forcing, and an increased positive longwave forcing. The RFO of the clear regime is not preserved between experiments, however, as can be seen in Figure S1, the change of the clear-sky RFO is only −0.1% from present-day to preindustrial conditions.

This effect is most visible in the midlevel cloud, where the forcing patterns in the thin and thick midlevel cloud regimes map onto each other fairly well. This indicates that for midlevel clouds, HadGEM3 predicts that the increased anthropogenic emissions are not causing a fundamental shift in which types of cloud are predominant over a given area, but merely an optical thickening of the pre-existing clouds, causing a shift from thin midlevel to thick midlevel clouds. As can be seen from Table S1, these two regimes primarily differ by α ($\Delta\alpha = 0.273$, c f. $\Delta\mathrm{CF} = 0.082, \Delta\mathrm{CTP} = 70\mathrm{hPa}$).

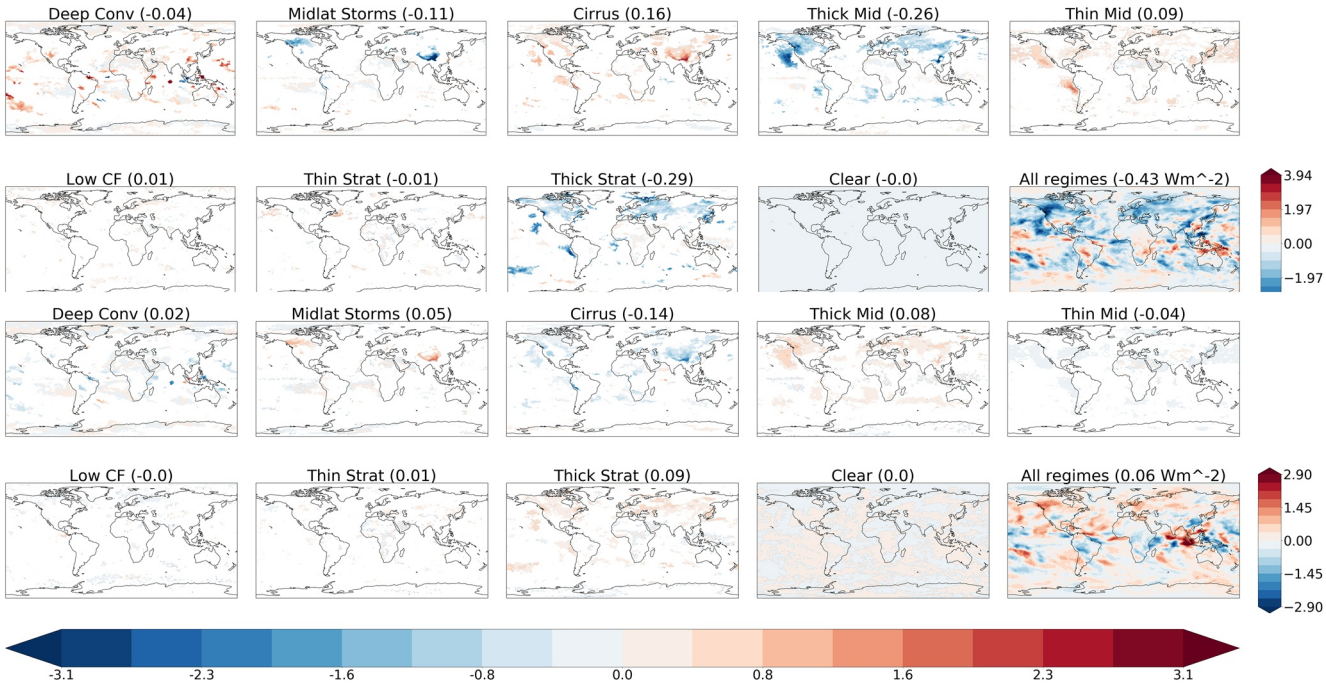

Figure 5. Indirect aerosol forcing arising from changes in RFO of each regime, $\Delta C^k_{\mathrm{RFO}}$. Colorbars are as in Figure 4.

The cirrus regime shows strong effects arising from regime transitions, which is not seen in the effects shown in Figure 4. This can be attributed to a strong decrease in the RFO of the cirrus regime over land and most of the Pacific Ocean (see Figure S1).

Two regimes neglected in discussion so far have been the deep convective and midlatitude storm regimes. The reason for this is that the aerosol scheme in HadGEM does not interact directly with the convection scheme, meaning that theoretically there should be no change in the properties of convective clouds between the two simulations. However, there are indirect interactions between the two schemes, and this means that while the forcing produced by these regimes are not attributable to noise, these figures may not be reliable and a specific experiment must be run to accurately diagnose the forcing for the convective regimes. In these simulations, the deep convective regime contributes a total of $-0.08\ \mathrm{Wm}^{-2}$ to the global indirect aerosol forcing.

The nonlinear effect, $\Delta R^k \Delta C^k$, is $\mathcal{O}(0.01\mathrm{Wm}^{-2})$ and so generally is not a dominant contribution to the overall forcing. The one exception to this is the cirrus regime, which exhibits $-0.06\ \mathrm{Wm}^{-2}$ to the global forcing via nonlinear effects. This, however, almost cancels out the linear effects shown by the cirrus regime, such that it only contributes $-0.02\ \mathrm{Wm}^{-2}$ to the global forcing.

4. Conclusions

Quantifying effective radiative forcing due to aerosol-cloud interactions remains a largely uncertain process, and the magnitude remains unconstrained in general circulation models. Previous studies focus on the magnitude of $\mathrm{ERF}_{\mathrm{ACI}}$ arising from all cloud types, however, here the $\mathrm{ERF}_{\mathrm{ACI}}$ from the HadGEM3-GA7.1 global climate model is decomposed into several global observational cloud regimes.

Simulated $\mathrm{ERF}_{\mathrm{ACI}}$ was broken down into contributions from a set of 10 observational cloud regimes using the methodology of Williams and Webb (2009). This is further broken down into both shortwave and longwave effects, and into two contributions with physically understandable definitions. This regime methodology has the key limitation of only being available on daylit points due to technical limitations of COSP, however, this has the advantage that the results can be easily compared with satellite data as a result of the design goal of COSP. Other regime classification methods exist, however, for instance Unglaub et al. (2020), which uses cloud base

height, and cloud top height variability to classify clouds from CALIPSO and CloudSat. This has the advantage of not being limited to daytime data and the disadvantage of sparse spatio-temporal sampling.

From this analysis it can be concluded that a large majority of forcing in the HadGEM3 GA7.1 comes from changes to the thick stratocumulus and thick midlevel cloud regimes (amounting to a total of −0.51 and −0.23 Wm^{-2}, respectively). These two sets of regimes have a similar geographical distribution and there may be some crossover between the two regimes, owing to the simplicity of the regime assignment method.

There is a lesser contribution from the low CF regime, which contributes −0.07 Wm^{-2} to the global ERF_{ACI}. This means that efforts should be focused on constraining the forcing produced specifically by these cloud regimes.

Comparing Figure 3 with the forcing plots, it can be inferred that the sensitivity of ERF_{ACI} to an increased aerosol loading is much greater in marine stratocumulus than in similar clouds seen over land.

The Cirrus regime shows strong individual effects that largely cancel each other out, however, these values must be taken with caution due to the lack of aerosol-ice interactions in the model. These large effects highlight the uncertain nature of ERF_{ACI} arising from ice clouds in GCMs and should encourage model developments to reduce the magnitude of uncertainty surrounding ERF_{ACI} from ice clouds.

The lack of correlation between the CCN perturbation and the total cloud forcing (seen in Figures 3 and S3 respectively) is the motivation for a detailed study of cloud sensitivities. The results of this study suggest that marine clouds are much more sensitive to aerosol perturbations than clouds seen over land.

This new tool can be used to gain insights into model representations of ERF_{ACI}. It is unclear whether the stratocumulus dominated ERF_{ACI} is a feature of all modern GCMs or whether aerosol-cloud interactions manifest themselves differently between different models, and this will be the topic of ongoing research.

Data Availability Statement

Raw simulation output data from the HadGEM3 model runs are available in the Met Office postprocessing data format (.pp; Met Office, 2013) from the JASMIN data infrastructure (http://www.jasmin.ac.uk) via the Met Office Managed Archive Storage System (MASS). The PI data are stored at moose:/crum/u-bg357/apk.pp and the PD data are stored at moose:/crum/u-bf393/apk.pp. Processed data used for all the results in this paper are publicly available at https://doi.org/10.5281/zenodo.4676264. The clusters used in this analysis were generated by George Tselioudis, William Rossow, Yuanchong Zhang, and Dimitri Konsta, and were made available for use at http://crest.ccny.cuny.edu/rscg/products.html.

Acknowledgments
This work was supported by the Natural Environment Research Council (grant number NE/RO11885/1). Philip Stier and Duncan Watson-Parris acknowledge funding from NERC projects NE/L01355X/1 (CLARIFY) and NE/P013406/1 (A-CURE). Philip Stier additionally acknowledges support from the ERC project RECAP and the FORCeS project under the European Union's Horizon 2020 research programme with grant agreements 724602 and 821205, respectively. Jane P. Mulcahy was supported by the Met Office Hadley Centre Climate Programme funded by BEIS and Defra (GA01101).

References

Abdul-Razzak, H., & Ghan, S. J. (2000). A parameterization of aerosol activation: 2. Multiple aerosol types. *Journal of Geophysical Research: Atmosphere*, *105*(D5), 6837–6844. https://doi.org/10.1029/1999jd901161

Albrecht, B. A. (1989). Aerosols, cloud microphysics, and fractional cloudiness. *Science*, *245*(4923), 1227–1230. https://doi.org/10.1126/science.245.4923.1227

Anderberg, M. R. (2014). *Cluster Analysis for Applications: Probability and Mathematical Statistics: A Series of Monographs and Textbooks* (Vol. 19). Academic Press.

Bellouin, N., Quaas, J., Gryspeerdt, E., Kinne, S., Stier, P., Watson-Parris, D., & Stevens, B. (2020). Bounding global aerosol radiative forcing of climate change. *Reviews of Geophysics*, *58*(1), e2019RG000660. https://doi.org/10.1029/2019rg000660

Bodas-Salcedo, A., Webb, M. J., Bony, S., Chepfer, H., Dufresne, J.-L., Klein, S. A., et al. (2011). COSP: Satellite simulation Software for model assessment. *Bulletin of the American Meteorological Society*, *92*(8), 1023–1043. https://doi.org/10.1175/2011bams2856.1

Boucher, O., Randall, D., Artaxo, P., Bretherton, C., Feingold, G., Forster, P., & Zhang, X. Y. (2013). *Climate change 2013: The physical science basis. Contribution of working group I to the fifth assessment report of the intergovernmental panel on climate change* (pp. 571–657). Cambridge University Press.

Ghan, S. J. (2013). Estimating aerosol effects on cloud radiative forcing. *Atmospheric Chemistry and Physics*, *13*(19), 9971–9974. https://doi.org/10.5194/acp-13-9971-2013

Gryspeerdt, E., & Stier, P. (2012). Regime-based analysis of aerosol-cloud interactions. *Geophysical Research Letters*, *39*(21). https://doi.org/10.1029/2012gl053221

Hoesly, R. M., Smith, S. J., Feng, L., Klimont, Z., Janssens-Maenhout, G., Pitkanen, T., & Zhang, Q. (2018). *Historical (1750–2014) anthropogenic emissions of reactive gases and aerosols from the community emissions data system (CEDS)* (Vol. 11). Geoscientific Model Development (Online). https://doi.org/10.5194/gmd-11-369-2018

IPCC (2013). Summary for policymakers. In T. F. Stocker, D. Qin, & G.-K. Plattner, (Eds.), *Climate change 2013: The physical science basis. Contribution of working group I to the fifth assessment report of the intergovernmental panel on climate change* (pp. 1–30). Cambridge University Press. https://doi.org/10.1017/CBO9781107415324.004

Jakob, C., & Tselioudis, G. (2003). Objective identification of cloud regimes in the tropical western Pacific. *Geophysical Research Letters*, *30*(21). https://doi.org/10.1029/2003gl018367

Mann, G. W., Carslaw, K. S., Spracklen, D. V., Ridley, D. A., Manktelow, P. T., Chipperfield, M. P., et al. (2010). Description and evaluation of GLOMAP-mode: A modal global aerosol microphysics model for the UKCA composition-climate model. *Geoscientific Model Development*, *3*(2), 519–551. https://doi.org/10.5194/gmd-3-519-2010

Mulcahy, J. P., Jones, C., Sellar, A., Johnson, B., Boutle, I. A., Jones, A., et al. (2018). Improved aerosol processes and effective radiative forcing in HadGEM3 and UKESM1. *Journal of Advances in Modeling Earth Systems*, *10*(11), 2786–2805. https://doi.org/10.1029/2018ms001464

Oreopoulos, L., Cho, N., & Lee, D. (2020). A global survey of apparent aerosol-cloud interaction signals. *Journal of Geophysical Research: Atmosphere*, *125*(1), e2019JD031287. https://doi.org/10.1029/2019jd031287

Rossow, W. B., & Schiffer, R. A. (1999). Advances in understanding clouds from ISCCP. *Bulletin of the American Meteorological Society*, *80*(11), 2261–2287. https://doi.org/10.1175/1520-0477(1999)080<2261:aiucfi>2.0.co;2

Rotstayn, L. D. (1999). Indirect forcing by anthropogenic aerosols: A global climate model calculation of the effective-radius and cloud-lifetime effects. *Journal of Geophysical Research*, *104*(D8), 9369–9380. https://doi.org/10.1029/1998jd900009

Schuddeboom, A., McDonald, A. J., Morgenstern, O., Harvey, M., & Parsons, S. (2018). Regional regime-based evaluation of present-day general circulation model cloud simulations using self-organizing maps. *Journal of Geophysical Research: Atmosphere*, *123*(8), 4259–4272. https://doi.org/10.1002/2017jd028196

Tselioudis, G., Rossow, W., Zhang, Y., & Konsta, D. (2013). Global weather states and their properties from passive and active satellite cloud retrievals. *Journal of Climate*, *26*(19), 7734–7746. https://doi.org/10.1175/jcli-d-13-00024.1

Twomey, S. (1977). The influence of pollution on the shortwave albedo of clouds. *Journal of the Atmospheric Sciences*, *34*(7), 1149–1152. https://doi.org/10.1175/1520-0469(1977)034<1149:tiopot>2.0.co;2

Unglaub, C., Block, K., Mülmenstädt, J., Sourdeval, O., & Quaas, J. (2020). A new classification of satellite-derived liquid water cloud regimes at cloud scale. *Atmospheric Chemistry and Physics*, *20*(4), 2407–2418. https://doi.org/10.5194/acp-20-2407-2020

Walters, D., Baran, A. J., Boutle, I., Brooks, M., Earnshaw, P., Edwards, J., et al. (2019). The Met Office Unified Model global atmosphere 7.0/7.1 and JULES global land 7.0 configurations. *Geoscientific Model Development*, *12*(5), 1909–1963. https://doi.org/10.5194/gmd-12-1909-2019

West, R. E. L., Stier, P., Jones, A., Johnson, C. E., Mann, G., Bellouin, N., et al. (2014). The importance of vertical velocity variability for estimates of the indirect aerosol effects. *Atmospheric Chemistry and Physics*, *14*(12), 6369–6393. https://doi.org/10.5194/acp-14-6369-2014

Williams, K. D., & Webb, M. J. (2009). A quantitative performance assessment of cloud regimes in climate models. *Climate Dynamics*, *33*(1), 141–157. https://doi.org/10.1007/s00382-008-0443-1

Wilson, D. R., & Ballard, S. P. (1999). A microphysically based precipitation scheme for the UK Meteorological Office Unified Model. *Quarterly Journal of the Royal Meteorological Society*, *125*(557), 1607–1636. https://doi.org/10.1002/qj.49712555707

Wilson, D. R., Bushell, A. C., Kerr-Munslow, A. M., Price, J. D., & Morcrette, C. J. (2008). PC2: A prognostic cloud fraction and condensation scheme. I: Scheme description. *Quarterly Journal of the Royal Meteorological Society*, *134*(637), 2093–2107. https://doi.org/10.1002/qj.333

Reference From the Supporting Information

Rossow, W. B., Walker, A. W., Beuschel, D. E., & Roiter, M. D. (1996). *International satellite cloud Climatology project (ISCCP) documentation of new cloud datasets (WMO/TD-No. 737)* (p. 115). World Meteorological Organization.